

QUANTIFYING POST-FIRE PONDEROSA PINE SNAGS USING GIS  
TECHNIQUES ON SCANNED AERIAL PHOTOGRAPHS

By Kevin Kent

A Thesis

Submitted in Partial Fulfillment  
of the Requirements for the Degree of  
Master of Science  
in Applied Geospatial Science

Northern Arizona University

December 2015

Committee:

Erik Schiefer, Ph.D., Chair

Mark Manone, M.A.

John Paul Roccaforte, M.S.

## **ABSTRACT**

### **QUANTIFYING POST-FIRE PONDEROSA PINE SNAGS USING GIS TECHNIQUES ON SCANNED AERIAL PHOTOGRAPHS**

Kevin Kent

Snags are an important component of forest ecosystems because of their utility in forest-nutrient cycling and provision of critical wildlife habitat, as well as associated fuel management concerns relating to coarse woody debris (CWD). Knowledge of snag and CWD trajectories are needed for land managers to plan for long-term ecosystem change in post-fire regimes. This need will likely be exacerbated by increasingly warm and dry climatic conditions projected for the U.S. Southwest. One of the best prospects for studying fire-induced landscape change beyond the plot scale, but still at a resolution sufficient to resolve individual snags, is to utilize the available aerial photography record. Previous field-based studies of snag and CWD loads in the Southwest have relied on regional chronosequences to judge the recovery dynamic of ponderosa pine (*Pinus ponderosa*) burns. This previous research has been spatially and temporally restricted because of field survey extent limitations and uncertainty associated with the chronosequence approach (i.e., space-for-time substitution), which does not consider differences between specific site conditions and histories.

This study develops highly automated methods for remotely quantifying and characterizing the spatial and temporal distribution of large snags associated with severe forest fires from very high resolution (VHR) landscape imagery I obtained from scans of aerial photos. Associated algorithms utilize the sharp

edges, shape, shadow, and contrast characteristics of snags to enable feature recognition. Additionally, using snag shadow length, image acquisition time, and location information, heights were estimated for each identified snag.

Furthermore, a novel solution was developed for extracting individual snags from areas of high snag density by overlaying parallel lines in the direction of the snag shadows and extracting local maxima lines contained by each snag polygon.

Field survey data coincident to imagery coverage for post-fire ponderosa pine forests allowed calibration and accuracy assessment of these new tools. These new methods may allow for broader estimation of snag dynamics in post fire landscapes while significantly lowering the human and material costs of conducting such surveys.

Outcomes for these methods were mixed. Both the snag count and snag height values were chronically underestimated using a feature extraction method and an edge detection method; so, an adjustment constant was developed for the categories of each method. Average accuracies ranged from 54 to 46% lower than the field-based values for the count attribute and 2-12% over the ground values for the snag height attribute using these two approaches. These methods show much promise, and are less resource intensive than field surveys, but more research is needed to improve overall accuracy.

Keywords: Snags, Coarse Woody Debris, Feature Detection, GIS, Aerial Photography, Edge Detection.

## **Acknowledgments**

To Carol Chambers and Joy Mast, who provided original ground survey data from their plots in the Pumpkin Fire burn area.

To the Joint Fire Science Program, whose funding through a Graduate Research Innovation grant (project ID: 13-3-01-28) allowed me to complete and expand this work.

To the fellow grad students in my cohort who provided useful feedback in our brainstorming sessions.

To my committee members Erik Schiefer, Mark Manone, and JP Roccaforte for their time, constructive input, and help along the way.

And most of all to my advisor Erik Schiefer who this would not have been possible without. His invaluable knowledge, expertise, wisdom, support, and patience was much appreciated.

## **TABLE OF CONTENTS**

<b>Abstract</b>	<b>ii</b>
<b>Acknowledgments</b>	<b>iv</b>
<b>Preface</b>	<b>vi</b>
<b>Introduction</b>	<b>1</b>
<b>Literature Review</b>	<b>4</b>
<b>Materials and Methods</b>	<b>11</b>
<b>Discussion</b>	<b>18</b>
<b>Conclusion</b>	<b>24</b>
<b>References</b>	<b>26</b>
<b>Figures</b>	<b>39</b>
<b>Tables</b>	<b>33</b>
<b>Appendices</b>	<b>35</b>

## **Preface**

This thesis is original, unpublished work created wholly by the author. This document is composed in a Journal format using the style consistent with its expected publication's guidelines, those of the Journal of Applied Remote Sensing, published by SPIE, the International Society for optics and photonics. This journal was chosen as the target for publication based on its relevance to the research in remote sensing. In preparation for this publication, the format of this thesis matches the required format of the journal for references, citations, and figures and tables are included outside of the body of text. To further prepare for publication some preliminary pages will need to be removed, acknowledgements will be moved to the end, a cover letter will be added, the literature review and introduction will be condensed, and other sections will be greatly condensed to reach the 4000 word limit.

## Introduction

Snags, or dead standing trees, are an important part of forest ecosystems, yet data on volume, and density are hard to come by (Ganey and Vojta 2012).

In recent decades in the southwestern United States, fires have become larger and more severe because of changes to climate and impact of past forest management methods (Haslem et al. 2011). Recent studies have suggested that contemporary burning is altering some regional ecosystems enough that ponderosa pine (*Pinus ponderosa*) forests are failing to regenerate even decades after severe crown fires (Savage and Mast 2005, Roccaforte et al. 2012).

Scientific- and management-related concerns associated with this ecological change range from the loss of important forest carbon sinks (Dore et al. 2008), to maintaining critical wildlife habitat (Chambers and Mast 2005), to concerns over reburning of areas due to heavy loads of standing and fallen snags (Passovoy and Fulé 2006). Roccaforte et al. (2012) emphasized that knowledge of snag trajectories is needed for land managers to plan for long-term ecosystem changes in the post-fire regimes. Furthermore, this need may be exacerbated by an increasingly warm and dry climate during the 21<sup>st</sup> century, which is associated with the increasing number of severe forest fires (Seager and Vecchi 2010).

In areas where they have been studied, snags exhibit large spatial and temporal variability (Morrison and Raphael 1993). Previously, studies of snags have relied on resource and time intensive ground surveys that have been necessarily limited in spatial extent (Passovoy and Fulé 2006). This research tests remote methods for measuring number and height of snags in post wildland fire ponderosa pine forests. Remote methods are unlikely to be as accurate as

ground surveys, but the tradeoffs could make them highly appealing in many situations. Such methods can use existing photographic and digital image resources, are less costly and time consuming than ground surveys, and can be scaled up to provide greater measurement capabilities at the landscape scale.

Remote sensing provides a significant opportunity for alternative methods to measure snags in a post-fire forest system. Light detection and ranging (LiDAR) is one obvious method for achieving this (Martinuzzi et al. 2009), but may be cost prohibitive and relatively complicated to use (Laes et al. 2006). The existing aerial photography record provides a unique approach because it is relatively affordable, already has widespread spatial and temporal coverage in many areas, and requires less technical expertise. Furthermore, it is likely the only approach available for providing historical measurements, potentially expanding back to the mid-20<sup>th</sup> century.

In this research, I developed an innovative new approach for estimating snag density and heights using aerial photos as the source data. Digital scans of existing large-scale analog aerial photos provided imagery of the study area and a feature extraction learning algorithm was applied to identify snag projected areas from their shadows, which are the most recognizable and distinct feature of snags in vertical aerial photos. Using novel methods, I developed an algorithm to delineate individual snags from large and complex shapes. The time, date, and locations of the aerial photos were used to perform a trigonometric calculation estimating the height of each snag based on the length of its shadow. Finally, I compared the results to the ground survey data to provide adjustment factors to better estimate the site specific height of detected snags. This research was



conducted using ground plots from northern Arizona's 2000 Pumpkin Fire (5,970 ha), with study areas coincident to plots previously ground-surveyed in 2001 and 2003 (Chambers and Mast 2005), with this data used for calibration and ground validation. Furthermore, this method was tested against a manual digitization of snags and a generic edge detection model to assess the relative accuracy of each approach.

## **Literature Review**

### **Importance of Coarse Woody Debris**

Coarse Woody Debris (CWD) is the scientific term for any large dead wood in an ecosystem. The term CWD most commonly refers to fallen logs >10 cm in diameter measured at breast height (dbh) (Stevens, 1997). However, CWD can also include stumps and standing dead trees, which are known as snags. CWD contributes to a wide array of ecological processes, many of which have only recently been more extensively studied. These aspects include nutrient cycles (Trudell et al., 2004), morphology (Nakamura and Swanson, 2006), post-fire dynamics (Passovoy and Fulé, 2006; Roccaforte et al., 2012), wildlife habitat (Bütler and Schlaepfer, 2004), and carbon sequestration dynamics (Woodall and Liknes, 2008). Furthermore, the type (logs or snags) and quantity of CWD play separate roles in wildfire studies (Brown et al., 2003; Passovoy and Fulé, 2006).

Passovoy and Fulé (2006) specifically emphasize the importance of CWD quantity. The amount and dynamics of logs and snags affect many aspects of fire hazard, behavior, and effects. As the amount of CWD increases, the fire intensity increases and makes suppression more difficult. Ignition becomes easier as CWD becomes more rotten and dry, but emits less heat than non-decaying wood (Passovoy and Fulé 2006). CWD can escalate large fires by producing a high surface heat, which can severely damage the soil. As the fuel load increases, so does the damage potential. Higher CWD loads can create a larger pulse of heat into the soil, creating a negative long term impact because soil development is a slow process, taking up to decades to recover to pre-fire nutrient levels.

Huang et al. (2009) emphasize that the ability to understand and manage

the effects large fires has been impacted by the lack of broad scale data. Due to the lack of data, the distribution of post-fire CWD is not well incorporated into process-based ecological thought and models, resulting in little research quantifying CWD and other spatially complex patterns created by fire.

### Why Aerial Photos?

Coarse woody debris assessments have generally been performed using field studies which are labor-intensive, expensive, and limited in their use for estimating measurements at the landscape scale (Passovoy and Fulé, 2006; Roccaforte et al., 2012). In recent years, research examining the feasibility of remote sensing methods for inventorying CWD has increased. There have been attempts to combine multiple remote sensing methods to measure CWD; Huang et al. (2009), combined Airborne Synthetic Aperture Radar (AirSAR) and optical Airborne Visible/Infrared Imaging Spectrometer (AVIRIS) imagery, while Tuominen and Haakana (2005) combined Landsat TM imagery and high altitude aerial photographs to measure forest characteristics, including CWD.

Additionally, satellite imagery is limited by its resolution. For example, Landsat has a nominal ground sample distance of 30 m for multispectral bands. Also, products like DigitalGlobe's WorldView-3 are limited by US government-imposed constraints of 0.25 m resolution for commercial imagery (MarketWired, 2014).

More recently, many of these studies have focused on using LiDAR (Pesonan et al., 2008; Martinuzzi et al., 2009). While laser scanner sensing has achieved generally good results, the cost of obtaining data is prohibitive for many cases (Stoker et al., 2008). While some governments have begun to embrace

LiDAR, the scope of available data is limited. Unless the cost of obtaining LiDAR decreases significantly, the existing aerial photo record provides the most cost effective method for obtaining very high resolution (VHR) imagery suitable for inventorying CWD. In the United States, broad-scale aerial photos can be purchased from the USDA's Aerial Photography Field Office and scanned into digital files at a sub-meter pixel resolution at a cost much cheaper than performing field studies or contracting LiDAR acquisitions.

Furthermore, color aerial photos covering the United States are widely available with 100% coverage over multiple dates, with even more special project missions for every National Forest. Also, aerial photos are the only remote sensing method that can provide high-resolution historical imagery now exceeding over a half century. This is extremely important for researchers studying historical trends in CWD dynamics. In addition, aerial photos generally have high temporal precision, with missions being repeated over the same area often on an intra- to inter-decadal period through programs like the historical National Aerial Photography Program (NAPP) and the current National Agriculture Imagery Program (NAIP).

## Field Studies

Much of the genesis for the ideas that motivated this study lies in the research done by Passovoy and Fulé (2006) and Roccaforte et al. (2012). These two studies employed near identical techniques to inventory CWD loads in wildfire burned areas in Arizona. Passovoy and Fulé investigated post-fire fuel dynamics, the decay and fall of standing snags, and the accumulation of the

fallen CWD on the surface, to help inform decisions about post-fire management, especially with respect to potential future fire behavior and effects. They concluded that CWD reaches its peak around five years after a fire. They surveyed sites from seven high-severity crown fires in the previous 3-27 years. At each site, they sampled 30 15 x 6 m plots and calculated CWD by using 15-meter planar transects. Furthermore, they classified each snag into one of five categories, indicating its decay class. With these measurements, they were able to calculate CWD biomass using previously developed equations and coefficients for Southwestern ponderosa pine forests. Roccaforte et al. used similar methods sampled 14 sites from 11 different high-severity Arizona ponderosa pine dominated fires and concluded that CWD peaked 6-12 years after fires. They sampled 30, 90 x 90 m, plots at all but one site. While this is certainly a large sample, the total survey area for each of these sites is only 24 ha for each site, yet the fires ranged in size from 500 to 186,000 ha, clearly illustrating the drawback with ground surveys for measuring CWD at the landscape-scale,

Savage and Mast (2005) demonstrate the need for new ways to measure forest biometrics. By surveying the state of ten severely burned ponderosa pine forest fire sites in northern Arizona and New Mexico, they were able to assess recovery trajectories decades after the fire. They concluded that two general trajectories exist: a robust recovery to an unnaturally dense ponderosa pine forest or a deflection of recovery to another vegetation state. In addition, they described the biogeomorphic processes of forest regeneration following wildfires and the role wood debris plays in this process. In acknowledging the changing fire regime in Southwestern forests towards less frequent and severe crown fires

and the effects this is having on forest dynamics, they explored the causes as two pronged. One being largely based on climate change, tending towards warmer, dryer summers, the other being the effects of direct anthropogenic measures such as logging, planting, fire suppression, and landscape stratification. Their sampling was done across 10 southwestern fires, with a 1 x 2.5 km grid laid out near the center of each burn where 30, 10 x 10 m, plots were measured for each site. This is only a total measurement of 0.3 ha for each burn, while burn sizes ranged from 800 to 36,000 ha, again demonstrating the spatial limitation of field surveys.

### Similar Studies and Techniques

To date, most studies attempting delineation of individual trees from remote sensing imagery have focused on live, unburned habitats. Ardila et al. (2012) proposed a method using VHR imagery to delineate live deciduous trees in an urban setting. Their work relied heavily on color infrared (CIR) imagery to tell trees apart from each other, but they used a local maxima technique to delineate adjoining features. Their method for this relied on a pixel-region growing process suitable for round, deciduous tree crowns. Haara and Nevalainen (2002) studied the efficacy of using aerial data to delineate spruce trees and measure defoliation. They also utilized CIR imagery to analyze the scenes. Their measures for defoliation and tree count were inaccurate at the scale of individual trees, but achieved excellent accuracy at the stand-scale.

Bütler and Schlaepfer (2004) is the most similar study to my own published so far. Their research looked at unmanaged, but unburned, spruce

forests in Switzerland using VHR aerial photography. Using stereoscopic CIR photos, they attempted to quantify large snags. By scanning standard 23 x 23 cm (9-inch) high resolution (1:10,000 nominal scale) photographs they were able to achieve a mean resolution of about 50 cm per pixel. CIR photography has been used in forest applications for many years because it has distinct advantages. Vegetation does a much better job of reflecting near-infrared electromagnetic waves than those in the visible range. Bütler & Schlaepfer note that with CIR photography live, dying, and dead snags provide a very distinguishable spectral response. The main problem with using CIR photos is they are underrepresented in the historical photo record in the United States, with often multiple decades between any repeat CIR photography, if any exists at all, while standard color photo surveys have been done with often intra-decadal frequency for many areas. Their work did not rely on automated classification of snag features; rather, the snags were manually digitized in a geographic information system (GIS). Detecting small snags was difficult, with accuracy rates for snag detection dropping sharply for snags with dbh < 25 cm. However, they attributed this inaccuracy to small snags being covered by the canopy or surrounding trees. For detecting snags with few or no branches they had to rely entirely on the shadow, which was only a “fine dark line.” This highlights the difficulty in the available methods for detecting snags without branches, as many are created after high-severity fires, even when using CIR photography. Such snags appear only as a single point, especially if they are near the nadir of the aerial imagery. This becomes more complicated in dense stands where there can be canopy closure and terrain factors (i.e., variable slope angles and aspects).

Hung et al. (2012) have demonstrated the feasibility of using only visual spectrum images to delineate objects. They traded multispectral imagery for high resolution (20 cm per pixel) images gathered from an unmanned aerial vehicle. Their method for feature detection involved using position, geometry, and appearance (including shadow) coupled with a spectral classification to distinguish objects. Their research focused on identifying crowns of living trees, but their methods can be adapted inventory CWD.

The available literature relevant to this study highlights a few important points. CWD is an important component of forests that has wide-ranging small- and large-scale impacts. Aerial photos provide a relatively inexpensive avenue for using remote sensing to measure CWD, especially relative to LiDAR and field studies. Other studies have attempted to use different aerial imagery types to study forest and snag dynamics, and their methods provide important background on the efficacy of different remote sensing techniques. These methods have exposed inaccuracies in estimating snag heights and the need for use of correction coefficients to better estimate height.



## **Materials and Methods**

This research was conducted using two sites in the ponderosa pine forests of northern Arizona. The areas studied are located within the Pumpkin fire (2000) area on the Kaibab and Coconino National Forests north of Kendrick Peak, as shown in Figure 1. I relied on two plots that were surveyed by Chambers and Mast (2005) for testing the approaches developed by this study and assessing accuracy. These plots are located within high-severity burn patches with >95% tree mortality. Elevation ranges from 2300 to 2550 m generally flat surfaces ( <10% slope) and the plots consist of 50 x 200 m (1 ha) rectangles individually oriented to encompass as many high-severity patches as possible.

The aerial imagery source materials consist of digital scans of existing true color 1:12,000 United States Department of Agriculture (USDA) aerial photos scanned by the Aerial Photography Field Office (APFO) at 12 microns to give a resolution of approximately 0.18 meters per pixel. Of the three 1 ha Pumpkin fire plots studied by Chambers and Mast during June 2001, only two are covered by the high-resolution imagery taken after the Pumpkin fire, which was captured on August 25, 2001. Each plot is shown on two separate overlapping photos, resulting in four available scenes for study. To perform the feature extraction, I created a model using Textron System's Feature Analyst software for ESRI's ArcGIS. For the remainder of the analysis I used ArcGIS Desktop Advanced 10.1, including the Spatial Analyst extension developed also by ESRI and the Python 2.7 integrated development environment.

I based the delineation of snags around detecting their shadow across the

ground surface. With vertical air photos of high-severity burned ponderosa pine stands, many snags appear as little more than a single point on the imagery due to the straightness of the trunks and the lack of large branches while their shadows appear as distinct dark lines across the ground.

### Image Preparation

After obtaining images from the APFO, pre-processing was required. The high-resolution scans came as .TIFF files that were >2 GBs each. I first cropped the images to include only the area immediately surrounding the study sites. I then georeferenced the images using five to six control points for each plot which were obtained in the field using GPS. Control points consisted of distinct points identifiable on the ground and in the imagery such as metal water tanks, road intersections, culverts, and large, distinct, individual live trees. I used a spline or rubbersheet georeferencing function because global accuracy was largely irrelevant for this study while local accuracy was paramount. Finally, using GPS and bearing data from Chambers and Mast (2005), I reconstructed the plot areas in a GIS and overlaid them on the imagery.

### Feature Analyst Method

Using the feature extraction tool Feature Analyst, I developed a learning algorithm to automatically resolve snag features from the plots. After testing 229 different parameter configurations a simple double-pass learning method was deemed the most effective algorithm because it had the least amount of type-II error (error where areas lacking snags were identified as snag polygons) and

was visually validated as being the best. The algorithm worked by creating a training sample of snag features and using a simple feature extraction run twice over the scene while employing a minimum shape size and applying a smoothing filter. To improve processing time the extraction extent was kept to the plot area and produced run times of four to five minutes for this step. This configuration was saved as an exportable accelerated feature extraction (.afe) file that was subsequently used on the other scenes using the Feature Analyst software, to create a polygon shapefile showing snag features, as shown in Figure 2.

#### Edge Detection Method

To give perspective on the feature extraction method, I employed a simpler method of using edge detection on each of the four scenes. To do this, I rotated each image (using a degree input so they could be exactly rotated back after) so the snag shadows were vertically oriented. A gradient edge detection function was performed using ArcGIS Image Analysis followed by a majority filter, which reclassifies pixels based on what the majority of pixels in its neighborhood are, to reduce noise. The kernel size for the edge detection was 3x3 pixels, as shown in Figure 3. Next I used binary reclassification using visual evidence of natural breaks in the scene between snag and non-snag areas. The snag zones were expanded by one pixel in each direction to fill out patchy areas, the scene was rotated back to its original orientation, and the snag raster zones were then converted to polygons that, like in the Feature Analyst method, represent the location and length of each snag's shadow. Once this method was developed I was able to complete this process for a single scene in approximately seven to

ten minutes.

### Manual Digitization Method

In this method, I digitized the shadows of snags in each of the four scenes by drawing polylines in ArcGIS in a new shapefile on top of the existing georeferenced imagery. Snag were digitized as lines representing the center of a snag shadow from shadow base to peak. This manual drawing automatically includes the lengths of each shadow in the shapefile geometry. A new tool was also constructed using ArcObjects for Visual Basic to assist in the rapid digitization of snags while assigning each snag to a decay class. However, measuring decay class was left outside the scope of the final analysis due to the difficulties in accurately establishing it using the available imagery. Using the streamlined workflow it would take 20-25 minutes to digitize all the snag features (259 to 285 snags) visible in a given plot.

### Complex Polygons

In many cases, especially areas with a high density of snags, large complex polygons where many parallel snag features are joined by short bridges of non-snag features were created by the automated methods, as exemplified in Figure 4. These overlaps were caused by overlap in the shadows of large branches on the snags, exacerbated by mixed pixels. This posed a serious problem because there was not an easy way to automate the breaking of such complex polygons into separate features. With simple polygons representing a single snag, the longest midline can be converted to a polyline to estimate the length for each feature, but this was not possible with large, complex polygons.

Fortunately, I developed a novel solution to this problem that is one of the more exciting outcomes of this research.

### Fishnet Snag Detection

To overcome this hurdle of complex snag polygon shapes, a fishnet is constructed. A fishnet is a regular grid of polylines, in this case a dense array of columns but only one row, where the column spacing is half that of the average snag polygon width. The fishnet is rotated by the user to align columns to be parallel with the snag shadows, with the angle of rotation determining the sun's azimuth, and laid over the detected snag area polygons. To facilitate these steps, I wrote a Python script packaged as an ArcGIS toolbox tool to automate the delineation of snag features from all polygons, including the large complex ones, and to calculate the height of each snag (Appendix B and C). The script consists of an identity tool that attaches the polygon IDs to the fishnet lines and then iterates polygon by polygon, finding the longest line in each polygon and outputting these as snag polylines. In complex polygons, where it is clear to the human eye that the polygon consists of multiple snag features, it flags all the local spatial maxima (in terms of length) of the parallel fishnet lines in a polygon, as shown in Figure 5. After selecting all the flagged local maxima lines, the script exports them to a new shapefile showing the position of all the snag shadows detected with noise removed (i.e., lines shorter than a user specified minimum length, and lines that cannot be snags because they are simply too short even though they are local maxima inside their respective polygons).

## Height Calculation

With lines representing the shadow of each snag detected, the script then calculates an estimated height of each snag. This involves using the US Naval Observatory's Sun Altitude/Azimuth calculator website to determine the angle of the sun's elevation, based on the previously derived azimuth of the sun, the location (latitude and longitude) of the scene, and the date on which the imagery was captured (US Naval Observatory 2015). The angle of the sun is used as a script input and a simple trigonometric function is employed to calculate the height of each snag in the attribute table:

$$H = L * \tan(a)$$

Where H is the height of the snags, L is the length of the shadow, and  $a$  is the angle of the sun's elevation in degrees. Following this, a final snag count and snag height statistics are available for the scene by viewing the attribute table summary statistics.

## Adjustment

Similarly to Büttler and Schlaepfer (2004). I derived a correction coefficient by comparing the automated height measurements to the field survey data. It was readily apparent that all methods were underestimating the height of the snags so that many features (as much as 75% of possible snag lines in some scenes) were below the minimum height, disqualifying them from being counted. To alleviate this compounding problem, I performed a height adjustment protocol on the outputs from the Feature Analyst and edge detection methods. However, I did not adjust the height of the digitized snags because the number of snags

detected using this method was largely accurate and without short lines that were unlikely to be snags. Using field survey data from Chambers and Mast (2005), I found the minimum height of the surveyed snags for each plot after removing outliers (height outliers defined here as snags shorter than 1.5 inter-quartile ranges <the first quartile). In the initial output, the average height of all detected snags (n) larger than the minimum measured height was normalized to the average height of the largest n snags in the field survey data. I used this system because it was presumed the larger snags were detected with the greatest accuracy because they would have longer shadows and a larger basal area, so there would be fewer shadows encroaching and overlapping it.

To better explain this system the following example from the Feature Analyst method is described. Plot 1 had a minimum (outlier removed – values <1.5 interquartile ranges below quartile 1) field-surveyed height of 8.35 m. The remotely sensed data from scene A/Plot 1 initially had 40 snags 8.35 m or higher; with an average height of 10.37 m. The largest 40 snags (of 325 in total) in the field survey data have an average height of 17.57 m. Thus, a height adjustment factor of 1.69 ( $17.57/10.37 = 1.69$ ) was used on all the snag features in scene A, creating a new adjusted height for each snag in the attribute table, after which 176 snag features were >the minimum height threshold of 8.35 m.

## **Discussion**

### **Count and Height Accuracy**

After the initial analysis was complete, extracted snag data was compared to the field survey data from Chambers and Mast (2005), shown in Table 1. Automated snag detection ranged from 117 to 237 out of 328 field measured snags for Plot 1B and 125 to 176 of 283 snags for Plot 2B. Accuracy for each scene and method as a percentage of the field survey data is shown in Table 2. The average accuracy of each method is shown in Table 3. After adjusting the height of each snag, average heights estimated from the automated techniques were 2 to 12% >the field surveyed height and only detected 46 to 56% of the snags in each scene. Both the Feature Analyst and edge detection method grossly underestimated the number of snags in each scene but on average were relatively accurate at estimating height when using an adjustment, capturing 93 to 124% of the true height.

### **Discrete Matching and Manual Digitization Accuracy**

One more assessment was devised to test the accuracy of the snag height data estimated using the Feature Analyst and Edge detection methods on a one-to-one snag basis. Using positional data from Chambers and Mast's (2005) field survey, a point shapefile was created showing the location of each snag. Due to error introduced from imprecise location information, plot coordinates, imagery georeferencing, and general inaccuracy of the snag detection methods, it was impossible to compare output snags to their field counterparts on a one-to-one basis across entire scenes. However, some snag



polygons were spatially isolated and distinct in size or shape that they were visually identified as the same features as their field counterparts with a high degree of certainty. I identified 10 such pairs in each Feature Analyst and Edge Detection scene and the average height was compared to field data with results, shown in Table 4. On average, the unadjusted height was only slightly less accurate than the adjusted height, with the adjusted height overestimating the true height while the unadjusted height underestimated it. Furthermore, the Edge Detection method generally measured snag pairs 4-7% shorter than the Feature Analyst method, with only the discrete matching in scene D measuring more than the Feature Analyst derived heights. The overestimation of the adjusted snag heights makes sense here because many of the snags that were isolated enough for discrete matching often were larger than most snags in the scene, biasing the accuracy of this assessment towards larger, isolated snags.

As shown in Table 3, manual digitization provides a high degree of accuracy (84-95%) for estimating the total number of snags in a scene, but only moderately accurate and highly variable height estimates (46-81%).

## Limitations

While this research represents a significant first step for using remote sensing methods to inventory snags in post-fire settings, more work is needed to improve the accuracy and identify the limitations of remote surveys.

Broad-scale imagery (1:12,000 or greater) is necessary for resolving ponderosa pine snag features when using true color air photos. It was originally intended that this research would have a broader scope by using data from more

plots on multiple different fires, but the lack of suitable imagery precluded this. I also experimented with 12 micron scans of finer-scale 1:20,000 color air photos, but deemed them too coarse to be able to resolve individual snag features without resulting in a very low degree of accuracy. Higher-resolution scans are possible (e.g. 7-10 microns); however, this currently requires even more specialized photogrammetric scanners and begins to approach the grain size of the original film (Schiefer and Gilbert, 2007). This research is applicable to natively digital aerial photos that have pixel resolutions of 0.2 m or higher or scans that produce a similar nominal resolution.

The methods described here need to be tested on a greater number of post-fire sites. These should encompass sites of various forest type, maturity, density, burn severity, slope, and locations. Accuracy needs to be categorically tested for each snag class to determine how accurate these methods estimate different size snags. The process for calculating height from shadows needs to be compared with results from imagery taken at different times of the day and with a broader range of sun elevation angles.

The algorithm used by the Feature Analyst method, while promising, is limited in multiple ways. One limitation was with the source imagery, in addition to true color imagery, color-infrared images could greatly increase the accuracy in distinguishing snag features, especially when the ground cover is live vegetation. Furthermore, high resolution imagery would also make features clearer and more easily delineated.

The algorithm used by the feature analyst is also limited by the learning process. I developed the algorithm using a finite number of training sites. With

such an approach, it is difficult to capture the entire range of spectral signatures and more importantly, change in spectral signature across all shapes and sizes of target features. A future solution to this problem could entail including a machine learning algorithm that would build on its knowledge of how to recognize target features as it continues to be used. Another problem was that the algorithm was not able to use the imagery of the actual tree stem in conjunction with its shadow to improve feature detection. For example, in scene B, the site is far enough from the nadir of the air photo that standing snags appear to lean to the right, and in some cases these stems are very linearly visible, and not just small dots or very small polygons as they would appear if the camera lens was directly overhead, as shown in Figure 6. This created a constant angle of intersection between snags and their shadows across the scene. Due to overlap of features this was not always visible but could have been useful in cases where it was prominently displayed. Another problem with the algorithm was the inability to detect small, narrow features. In Figure 6 you can also clearly see individual snag shadows that were not detected, likely because they were too thin. Another problem was the combining of closely spaced features where two shadows were adjacent to each other, they were likely to be counted as one wide feature instead of two narrow side by side features. It might be possible to mitigate this by setting a maximum width for features, but it would be more useful to simply have higher resolution imagery.

One more issue is the difference in measurements between the two scenes for each plot, A vs B for plot 1 and C vs D for plot 2. The most likely reason for this is the difference in the position of each scene in their respective

photographs relative to the nadir of the image. This can cause snag trunks to appear to lean in different directions even though their shadows were consistent among between images. This can cause more or less overlap of snag polygon features, which changes the effectiveness of the algorithm.

The devised fishnet method for resolving individual snags from complex polygon features was feasible with horizontally bridged-together features, but is ineffective at separating snags whose shadows are vertically aligned (i.e. end to end) inside one polygon. A new approach at resolving this issue would be needed, perhaps by setting a relative length threshold for keeping two features on one line when appropriate

## Advantages

The main advantage of the methods tested in this research is the substantial savings in time and capital required to create estimates of post-fire snag data. Furthermore, this method is scalable and can be used to gain precise estimates on snags at the landscape level.

The novel fishnet delineation method allowed for delineating snags from complex polygons within high-density areas. By finding all the local maxima, instead of a fixed number of the longest lines in each shape, there was no theoretical limit to how complex a polygon could be and still resolve snags. While this was an important breakthrough, it was imperfect and more development is needed to resolve issues for vertical alignment of snag shadows.

## Implications

Clearly, remote methods for measuring forest structure dynamics, including post-fire snag data, is an important field for land managers to take interest in. With improvements in accuracy and broad scale testing of these methods, they can provide an inexpensive new tool for land managers and researchers to quickly and efficiently measure fire impacts. In an era of budgetary concerns and limits on human resources, remote sensing has the potential to significantly decrease data collection costs. Furthermore, remote sensing, and especially automated techniques, provides an important opportunity for greatly expanding the scale from which detailed forest data can be obtained, from the plot-level to the landscape-scale. As discussed earlier, LIDAR is another possible avenue for collecting such data (Martinuzzi et al. 2009), but traditional aerial photos are much more ubiquitous, less costly to obtain, and require less expert knowledge to analyze.

## **Conclusion**

Remote methods for inventorying post-fire snags can provide a way of estimating snag density and height in post-fire environments. The results among the different methods tested varied in accuracy but provide a strong starting point for investigating the use of aerial photos for creating estimates of number and height of snags in an area. These methods clearly need refinement and further, broader testing, but they have shown to provide promising results for use in the area in which they were developed. At the very least, this research is ready to provide snag number and height estimations that accurately predict snag density and height within the correct order of magnitude, which will be useful for land managers. Height measurements, in particular, and especially for large snags in open areas, provide a very promising avenue for future research uses, as they captured between 70 and 102% of the average field measured height for the plots in this study, even before any adjustments were made.

Furthermore, this research demonstrates how complex polygons encompassing multiple snags can be systematically manipulated to resolve individual snag features using the novel fishnet approach; however, this technique also needs further refinement and testing to improve it to a level where it is accurate enough for widespread adoption. The open-source fishnet automated script will additionally allow a wider body of researchers, including those who are less GIS savvy, a new user friendly tool for their use and a system that can be easily modified and improved upon.

Snags are an important, ecologically relevant component of forest diversity. Because current methods for estimating snag volumes require

expensive, labor- and time-intensive ground surveys, new remote survey methods can help bridge the information gap, especially when information is rapidly needed after large disturbances such as wildfires. This research can lay a foundation for more refined remote sensing methods to become a common measurement vehicle for land managers, researchers, and forest stakeholders.

## References

- Ardila, J.P., Bijker, W., Tolpekin, V.A., and Stein, A. 2012. Context-sensitive extraction of tree crown objects in urban areas using VHR satellite images. *International Journal of Applied Earth Observations*. 15: 57-69.
- Brown, J. K., Reinhardt, E. D., & Kramer, K. A. 2003. Coarse woody debris: managing benefits and fire hazard in the recovering forest. US Department of Agriculture, Forest Service, Rocky Mountain Research Station.
- Bütler, R., & Schlaepfer, R. 2004. Spruce snag quantification by coupling colour infrared aerial photos and a GIS. *Forest Ecology and Management*, 195, 325-339.
- Chambers C., and Mast, J. 2005. Ponderosa pine snag dynamics and cavity excavation following wildfire in northern Arizona. *Forest Ecology and Management* 216, 227–240.
- Dore, S., Kolb, T., Montes-Helu, M., Sullivan, B.W., Winslow, W.D., Hart, S.C., Kaye, J.P., Koch, G.W., and Hungate, B.A. 2008. Long-term impact of a stand-replacing fire on ecosystem CO<sub>2</sub> exchange of a ponderosa pine forest. *Glob. Change Biol.* 14, 1801-1820.
- Ganey, J. L., & Vojta, S. C. 2012. Rapid increase in log populations in drought-stressed mixed-conifer and ponderosa pine forests in northern Arizona. *Open Journal of Forestry* 2, 59-64.
- Ganey, J. L., & Vojta, S. C. 2012. Trends in Snag Populations in Drought-Stressed Mixed-Conifer and Ponderosa Pine Forests (1997–2007). *International Journal of Forestry Research*, 2012.
- Haara, A., & Nevalainen, S. 2002. Detection of dead or defoliated spruces using digital aerial data. *Forest Ecology and Management*, 160, 97-107.
- Haslem, A., Kelly, L., Nimmo, D., Watson, S., Kenny, S., Taylor, R., Avitabile, S., Callister, K., Spence-Bailey, L., Clarke, M., and Bennett, A. 2011. Habitat or fuel? Implications of long-term, post-fire dynamics for the development of key resources for fauna and fire. *J. Appl. Ecol.* 48, 247-256.
- Hung, C., Bryson, M., and Sukkarieh, S. 2012. Multi-class predictive template for tree crown detection. *ISPRS Journal of Photogrammetry*. 6, 170-183.
- Huang, S., Crabtree, R. L., Potter, C., & Gross, P. 2009. Estimating the quantity and quality of coarse woody debris in Yellowstone post-fire forest ecosystem from fusion of SAR and optical data. *Remote Sensing of Environment*, 113, 1926-1938.
- Laes, D., Warnick, R., Goetz, W., Maus, P. 2006. Lidar Application for Forestry



and Geosciences. Forest Service Remote Sensing Tips. RSAC-73-TIP1. Salt Lake City, UT: U.S. Department of Agriculture, Forest Service, Remote Sensing Applications Center.

MarketWired. 2014. U.S. Department of Commerce Relaxes Resolution Restrictions DigitalGlobe Extends Lead in Image Quality. June 11, 2014. Retrieved September 10, 2015, from <http://www.marketwired.com/press-release/us-department-commerce-relaxes-resolution-restrictions-digitalglobe-extends-lead-image-nyse-dgi-1919482.htm>.

Martinuzzi, S., Vierling, L. A., Gould, W. A., Falkowski, M. J., Evans, J. S., Hudak, A. T., & Vierling, K. T. 2009. Mapping snags and understory shrubs for a LiDAR-based assessment of wildlife habitat suitability. *Remote Sensing of Environment*, 113(12), 2533-2546.

Morrison, M., and Raphael, M. 1993. Modeling the dynamics of snags. *Ecological Applications*, 322-330.

Nakamura, F., & Swanson, F. J. 2006. Effects of coarse woody debris on morphology and sediment storage of a mountain stream system in western Oregon. *Earth Surface Processes and Landforms*, 18, 43-61.

Passovoy, M., and Fulé, P. 2006. Snag and woody debris dynamics following severe wildfires in northern Arizona ponderosa pine forests. *For. Ecol. Manage.* 223: 237-246.

Pesonen, A., Maltamo, M., Eerikäinen, K., & Packalén, P. 2008. Airborne laser scanning-based prediction of coarse woody debris volumes in a conservation area. *Forest Ecology and Management*, 255, 3288-3296.

Roccaforte, J.P., Fulé, P., Chancellor W., Laughlin, D. 2012. Woody debris and tree regeneration dynamics following severe wildfires in Arizona ponderosa pine forests. *Can. J. For. Res.* 42, 593-604.

Savage, M., and Mast, J. 2005. How resilient are southwestern ponderosa pine forests after crown fires? *Can. J. For. Res.* 35, 967-977.

Schiefer, E. and Gilbert, R. 2007. Reconstructing Long-Term Morphometric Change in a Proglacial Landscape Using Historical Aerial Photography and Automated DEM Generation. *Geomorphology*. 88, 167-178.

Seager, R., and Vecchi, G. 2010. Greenhouse warming and the 21st century hydroclimate of southwestern North America. *Proc. Natl. Acad. Sci. U.S.A.* 107, 21277-21282.

Stoker, J., Harding, D., & Parrish, J. 2008. The Need for a National Lidar Dataset. *Photogrammetric Engineering & Remote Sensing*, 1067.

- Stevens, V. 1997. The ecological role of coarse woody debris: an overview of the ecological importance of CWD in BC forests. British Columbia, Ministry of Forests, Research Program.
- Trudell, S. A., Rygiewicz, P. T., & Edmonds, R. L. 2004. Patterns of nitrogen and carbon stable isotope ratios in macrofungi, plants and soils in two old-growth conifer forests. *New Phytologist*, 164, 317-335.
- Tuominen, S., & Haakana, M. 2005. Landsat TM imagery and high altitude aerial photographs in estimation of forest characteristics. *Silva Fennica*, 39, 573.
- Woodall, C. W., & Liknes, G. C. 2008. Relationships between forest fine and coarse woody debris carbon stocks across latitudinal gradients in the United States as an indicator of climate change effects. *Ecological Indicators*, 8, 686-690.
- US Naval Observatory. 2015. Sun of Moon Altitude/Azimuth Table. Retrieved June 2, 2015, from <http://aa.usno.navy.mil/data/docs/AltAz.php>

## Figures

Figure 1. Study Site Location Map with plots and Pumpkin Fire.

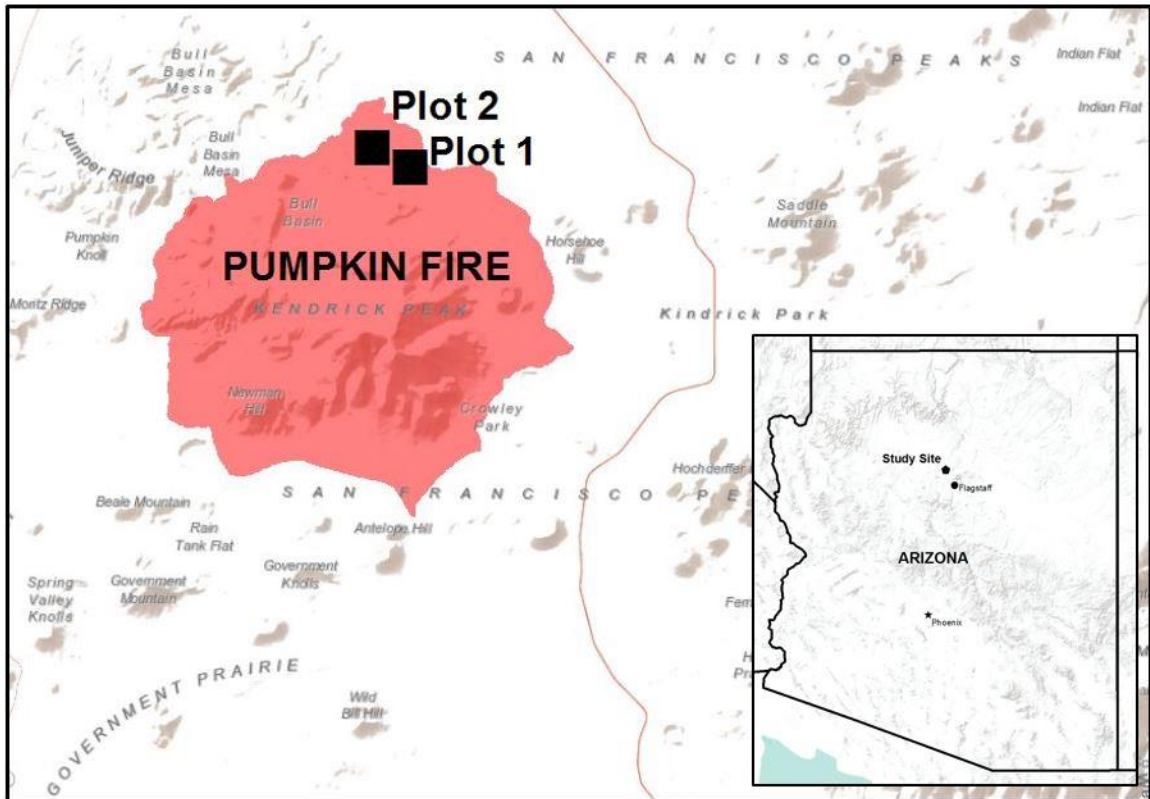


Figure 2. Feature Analyst snag polygons, scene A, plot 1. The black bounding box is the boundary of plot 1; the green shapes are the detected snag polygons.

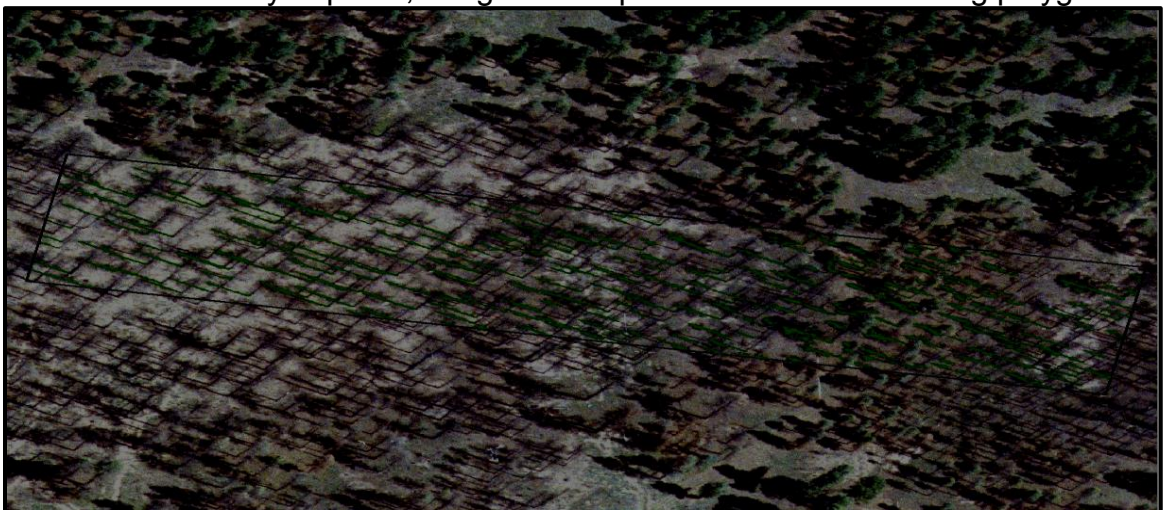


Figure 3. Gradient kernel configuration for Edge Detection method. This is the default edge detection kernel used by ArcGIS.

1	0	-1
2	0	-2
1	0	-1

Figure 4. Complex snag area polygon, highlighted in blue outline, scene D, plot 2. This shows one polygon on the edge of the plot (also blue line down the left side) that is clearly multiple different snags which are connected via short horizontal bridges, necessitating a way to break apart this polygon.

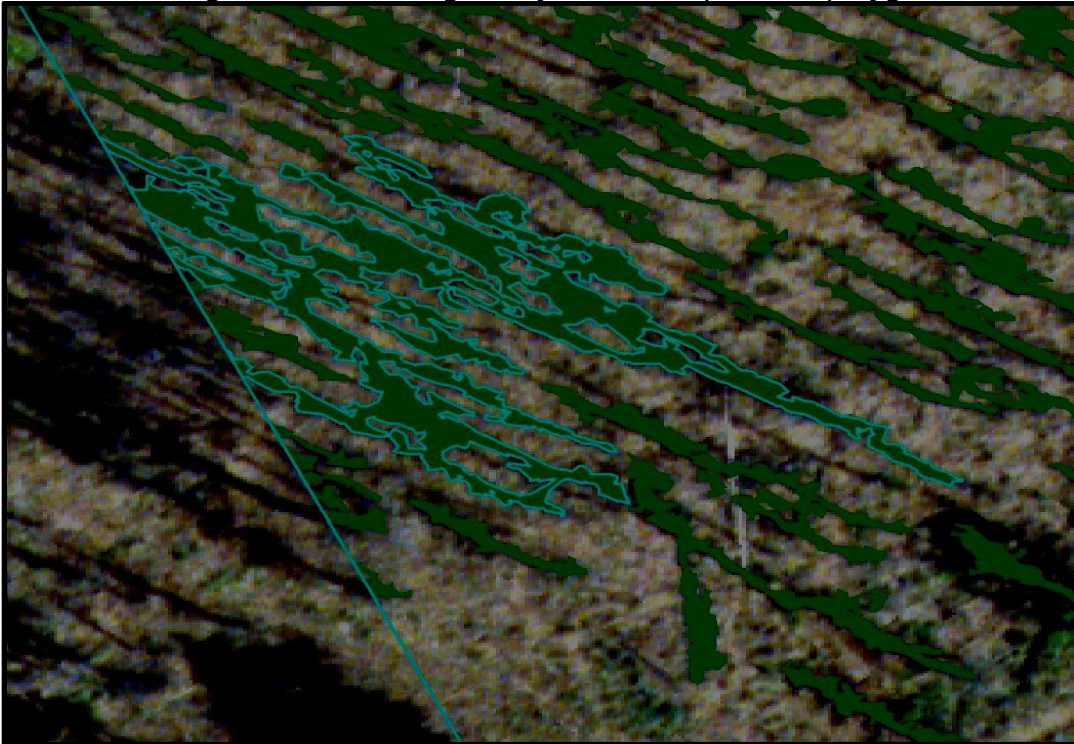




Figure 5. Complex polygon (light green) with snag features detected from fishnet local maxima (red lines). The rest of the detected polygons in the scene are shown as dark green polygons and the black line is the plot boundary. This is the same polygon from Figure 4, but here it shows the local maxima considered to be snag features.

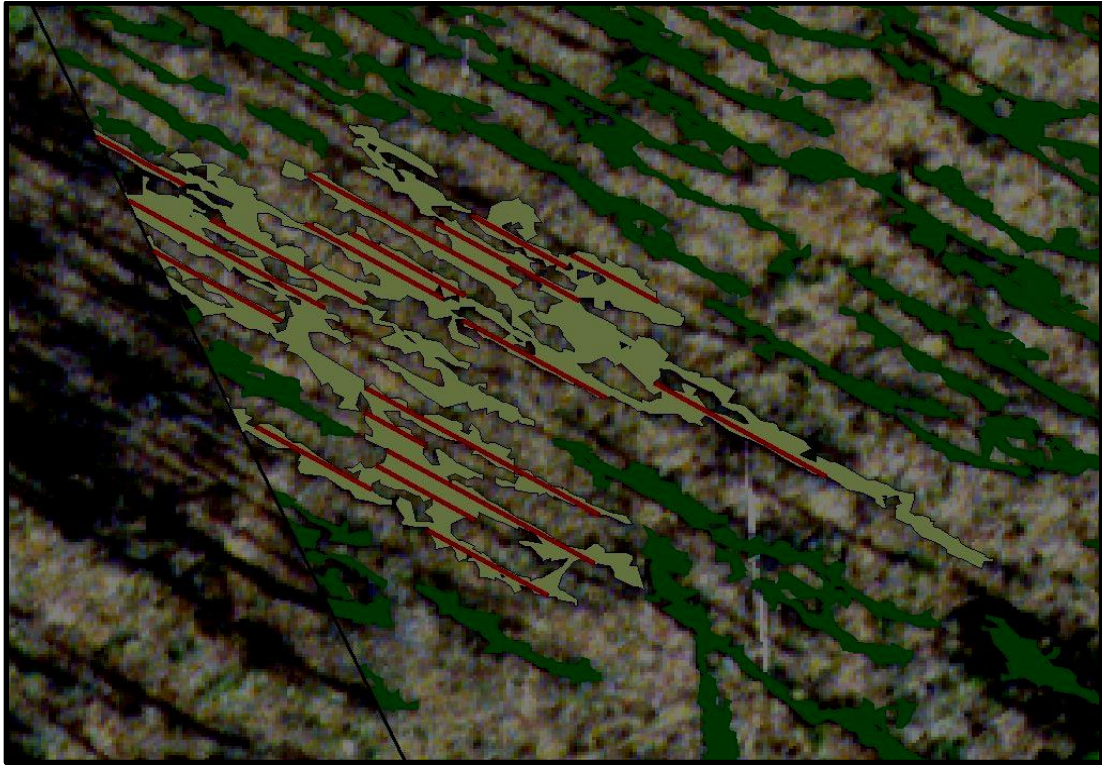
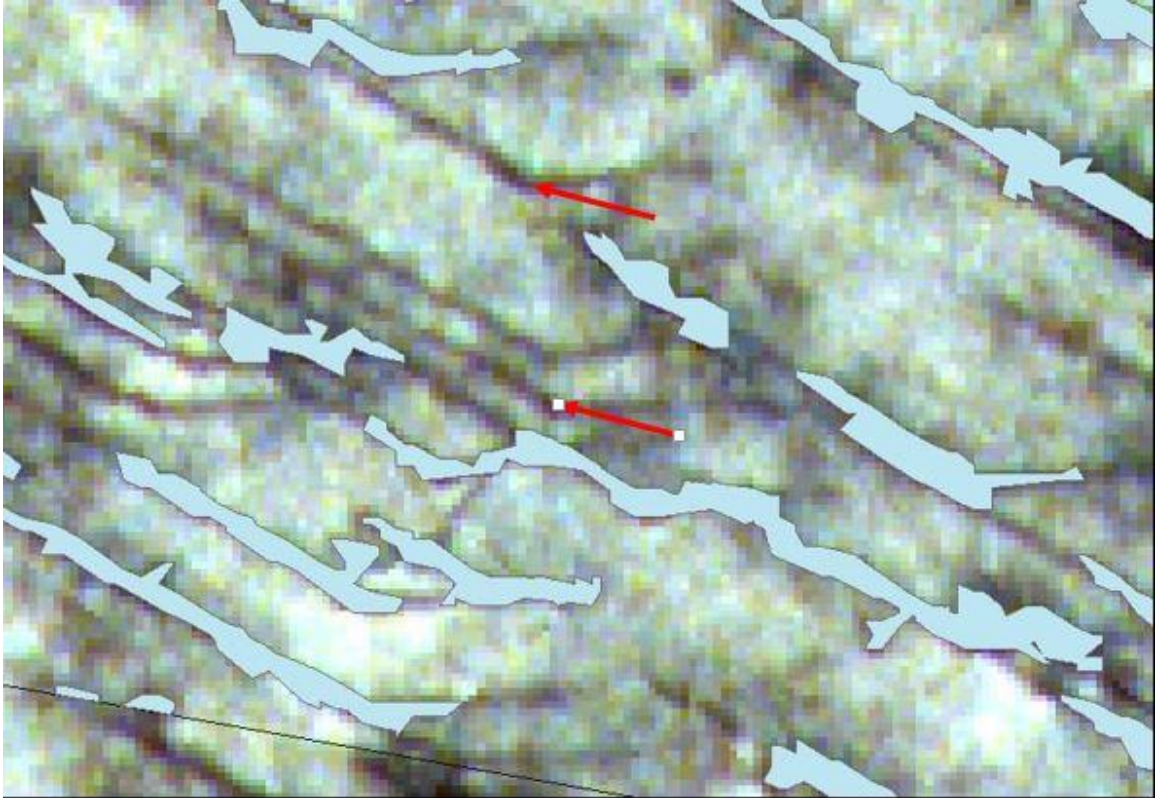


Figure 6. An example in scene B of how many snags (shown here as blue polygons) were not incorporated into the feature detection and how the algorithm did not detect narrow shadow. In the middle, marked by red arrows, there are two examples of snag shadows that were not detected. On the right side of the image there is a prominent example of the actual snag detected in one piece with its shadow



## Tables

Table 1. Results from Feature Analyst (\_FX), Edge Detection (\_ED), and Digitization Methods (\_DIG). The A, B, C, and D prefixes indicate which scene each result is from. This table shows how many snags taller than the minimum height, as found via the field survey, were originally detected using each method and their average height. By comparing predicted heights to the field height data, an adjustment was performed that increased the average height for each category and thus the number of qualifying snag features. Each plot is 1 ha in size, thus the number of snags is the same as density of snags/ha.

Plot	P1B						
Scene	A_FX	B_FX	A_ED	B_ED	A_DIG	B_DIG	Ground
UnAdj. Snags	40	51	135	141	285	277	328
UnAdj. Avg. Ht	10.4	11.3	11.3	18.4	10.7	10.8	13.3
Adj. Snags	176	117	237	141	X	X	X
Adj. Avg. Ht	12.3	13.4	13.9	16.5	X	X	X
Adj.Factor	1.69	1.53	1.47	0.90	X	X	X
Plot	P2B						
Scene	C_FX	D_FX	C_ED	D_ED	C_DIG	D_DIG	Ground
UnAdj. Snags	103	79	76	192	259	267	283
UnAdj. Avg. Ht	12.6	10.8	11.1	18.3	6.9	5.9	12.7
Adj.Snags	125	147	132	176	X	X	X
Adj. Avg. Ht	14.1	13.2	13.4	14.3	X	X	X
Adj.Factor	1.20	1.45	1.43	0.75	X	X	X

Table 2. . Accuracy of each method as a percentage of field data (\*digitization results unadjusted) from Feature Analyst (\_FX), Edge Detection (\_ED), and Digitization Methods (\_DIG). The A, B, C, and D prefixes indicate which scene each result is from.

Plot P1B						
Method	A_FX	B_FX	A_ED	B_ED	A_DIG*	B_DIG*
Adj. Count	53.7%	35.7%	72.3%	43.0%	86.9%	84.5%
Adj. Height	92.6%	101.1%	104.5%	124.3%	80.8%	81.3%
Plot P2B						
Method	C_FX	D_FX	C_ED	D_ED	C_DIG*	D_DIG*
Adj. Count	44.2%	51.9%	46.6%	62.2%	91.5%	94.3%
Adj. Height	110.7%	103.7%	105.7%	112.7%	54.1%	46.4%

Table 3. Average accuracy by method (\*digitization results unadjusted) as a percentage of field survey data for Feature Analyst (FX), Edge Detection (ED), and Digitization Methods (DIG).

Method	FX	ED	DIG*
Adj. Count	46.4%	56.0%	89.3%
Adj. Height	102.0%	111.8%	65.6%

Table 4. Average of one-to-one accuracy assessment from a discretely matched sample of 10 pairs of snags from the Feature Analyst derived height data, as a percentage of field data for Feature Analyst (\_FX) and Edge Detection (\_ED). The A, B, C, and D prefixes indicate which scene each result is from.

Plot	P1B			
Scene	A_FX	A_ED	B_FX	B_ED
UnAdj. Height	65.8%	61.7%	77.6%	75.8%
Adj.Height	111.2%	105.5%	118.8%	112.0%
Plot	P2B			
Scene	C_FX	C_ED	D_FX	D_ED
UnAdj. Height	101.8%	94.1%	80.0%	84.6%
Adj.Height	122.1%	118.4%	116.0%	121.1%



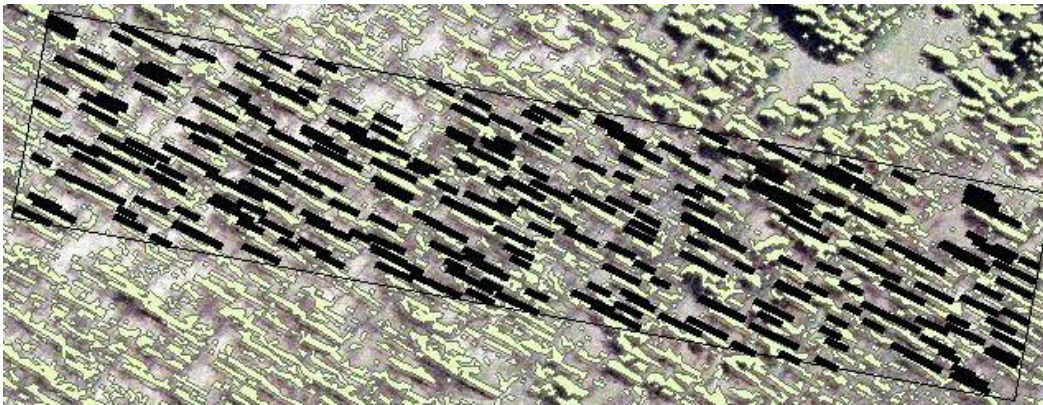
## Appendices

### Appendix A. Photos of each scene

Scene A\_FX. Black lines showing fishnet derived snags from local maxima and yellow polygons are snag polygons, using the feature extraction method on Scene A:

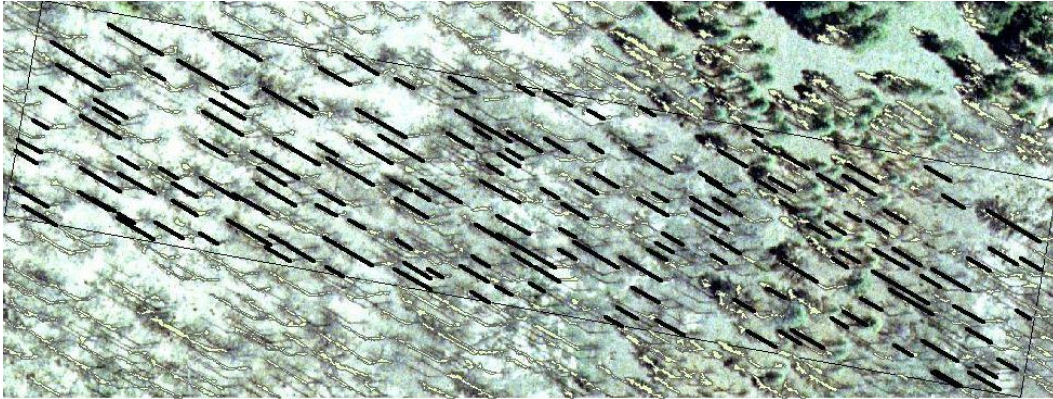


Scene A\_ED. Black lines showing fishnet derived snags from local maxima and green polygons are snag polygons, using the Edge Detection method on scene A:

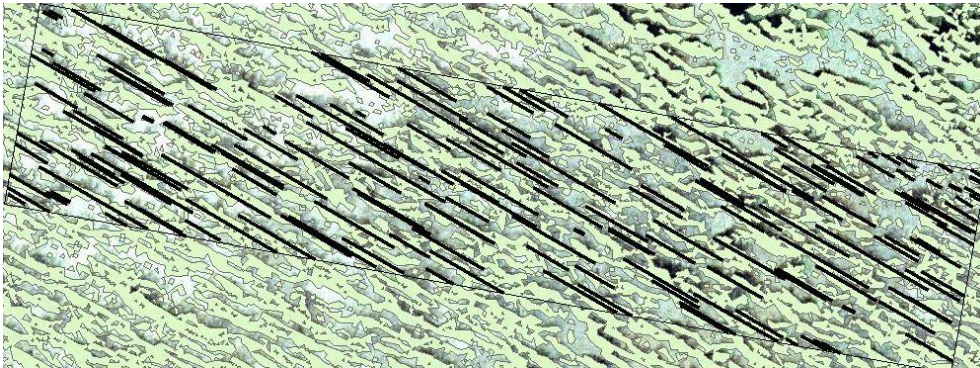


Scene B\_FX. Black lines showing fishnet derived snags from local maxima and yellow polygons are snag polygons, using the feature extraction method on Scene B:



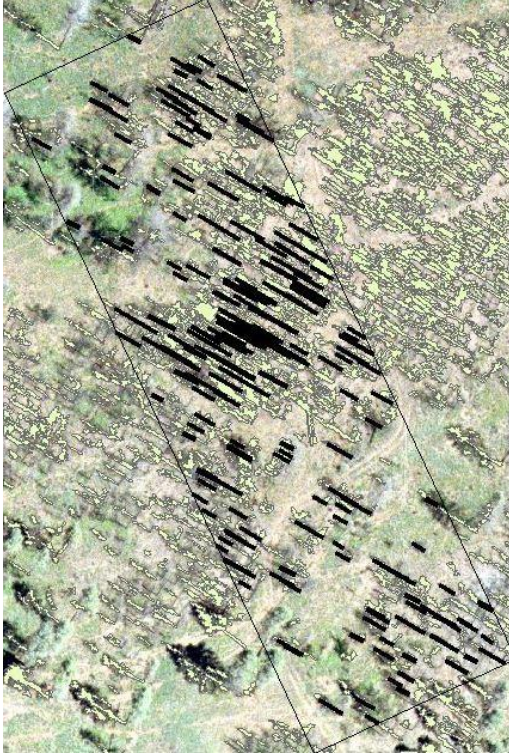


Scene B\_ED. Black lines showing fishnet derived snags from local maxima and green polygons are snag polygons, using the edge detection method on Scene B:

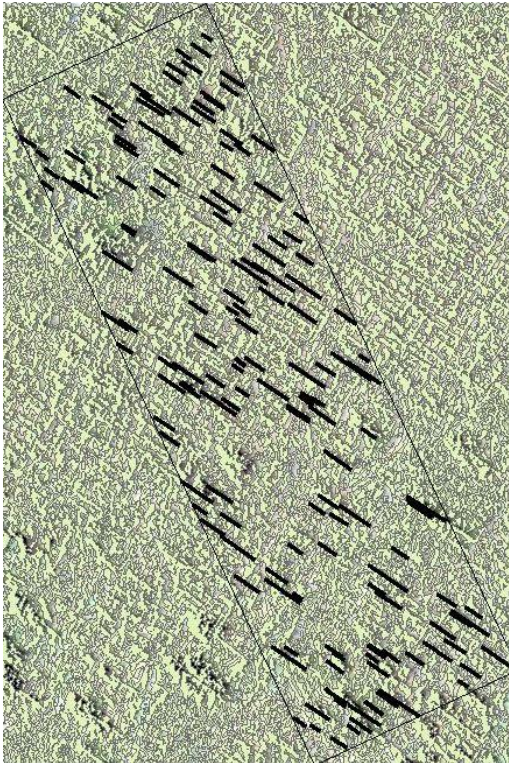


Scene C\_FX. Black lines showing fishnet derived snags from local maxima and yellow polygons are snag polygons, using the feature extraction method on Scene C:





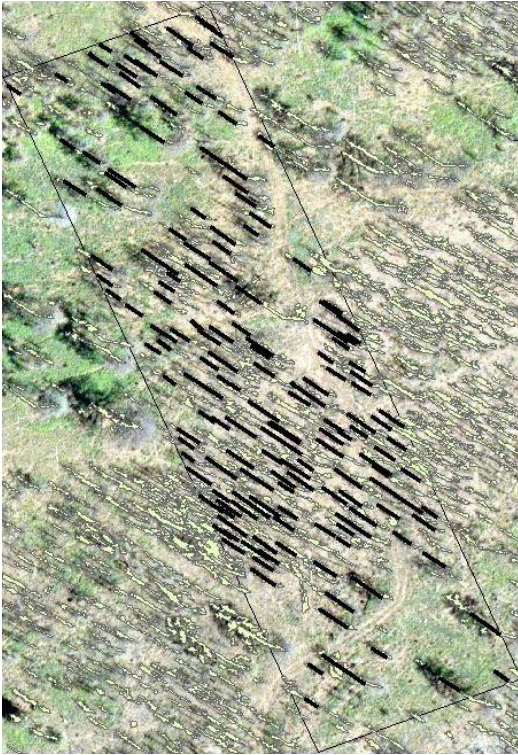
Scene C\_ED. Black lines showing fishnet derived snags from local maxima and yellow polygons are snag polygons, using the edge detection method on scene C:



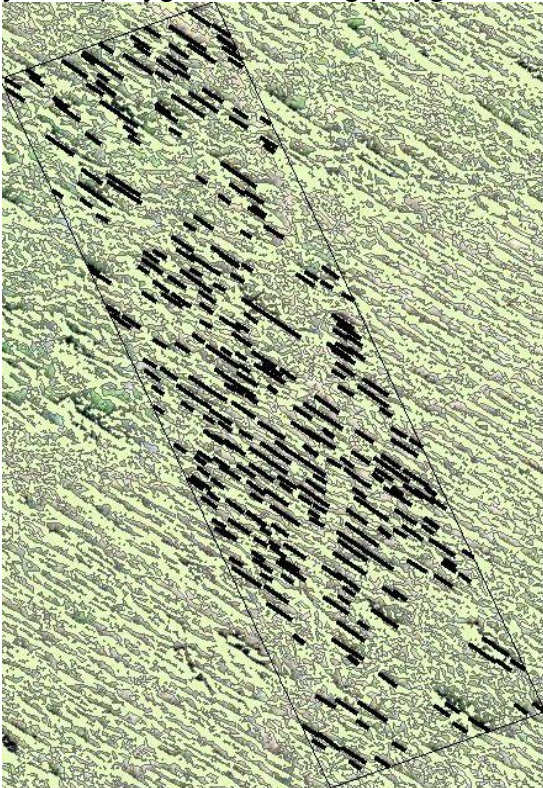
Scene D\_FX. Black lines showing fishnet derived snags from local maxima and yellow polygons are snag polygons, using the feature extraction method on



Scene D:



Scene D\_ED. Black lines showing fishnet derived snags from local maxima and yellow polygons are snag polygons, using edge detection method on Scene D:



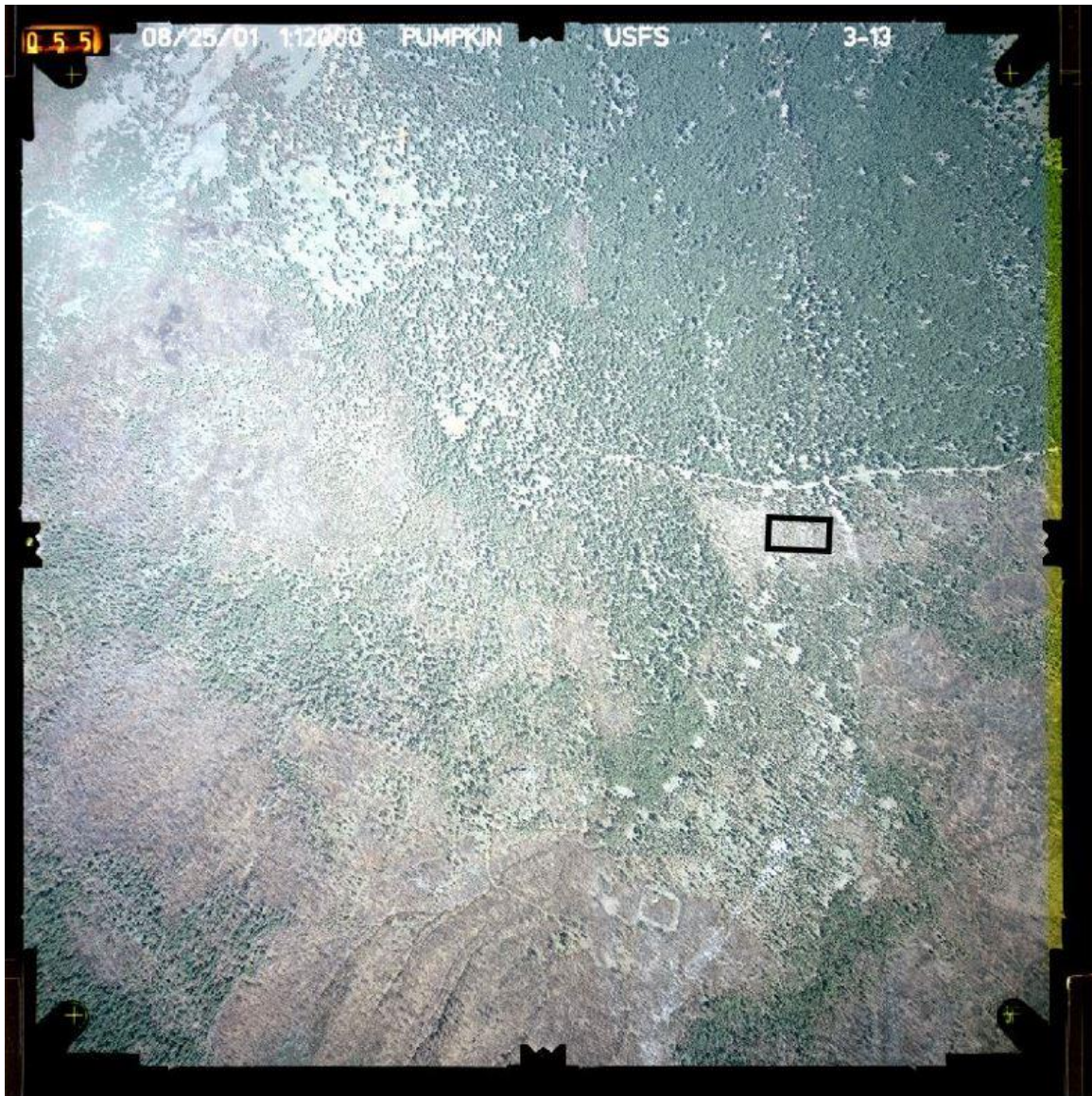


Scene A original aerial photo with Plot 1 (40° and 1200 meters from nadir) shown in the black box:





Scene B original aerial photo with Plot 1 (90° and 600 meters from nadir) shown in the black box:



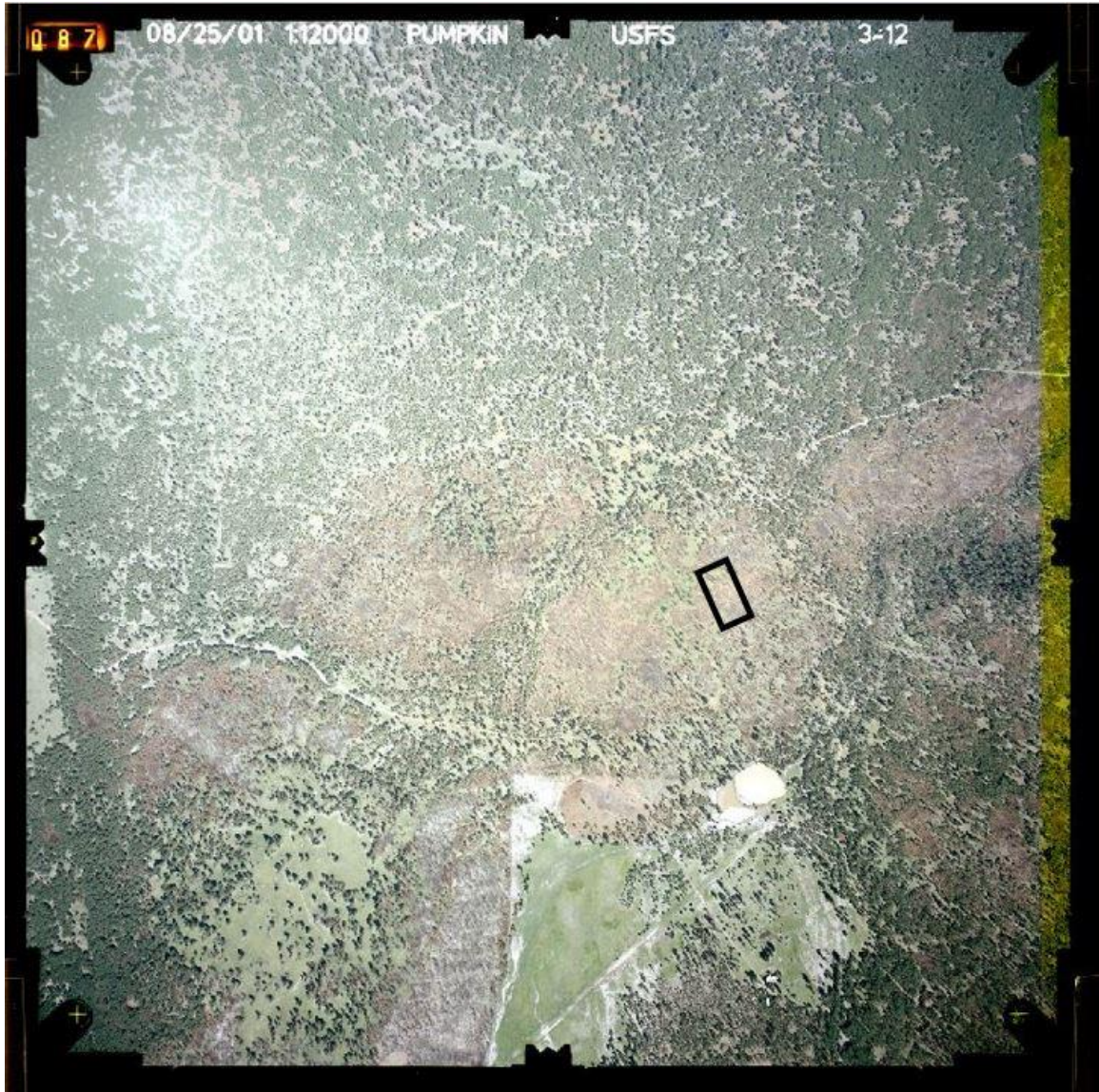


Scene C original aerial photo with Plot 2 (25° and 1000 meters from nadir) shown in the black box:





Scene D original aerial photo with Plot 2 (100° and 400 meters from nadir) shown in the black box:





## Appendix B. Python Script

### local\_maxima\_snag\_script.py

```
1.  ###This script finds the local maxima of fishnet lines by length that inter-
    sect polygons
2.  ###Written by Kevin Kent, Northern Arizona University
3.  ###Created to be used with "Find Longest Snags" script in Snag_Detec-
    tor.tbx ArcGIS Toolbox
4.  ###written for python 2.7
5.
6.  import os
7.  import arcpy
8.  import numpy as numpy
9.  import math
10.
11. # Set the inputs for workspace, polygon fc/shapefile, fishnet, and projection
12. arcpy.env.workspace = arcpy.GetParameterAsText(0)
13. polygon_input = arcpy.GetParameterAsText(1)
14. fishnet_input = arcpy.GetParameterAsText(2)
15. roi = arcpy.GetParameterAsText(3)
16. projection = arcpy.GetParameterAsText(4)
17. angle = float(arcpy.GetParameterAsText(5))
18. min_height = float(arcpy.GetParameterAsText(6))
19.
20. #set workspace variable
21. workspace = arcpy.env.workspace
22.
23. #allow overwriting
24. arcpy.env.overwriteOutput = True
25.
26. #create scratch folder
27. arcpy.CreateFolder_management(workspace, "intermediate_outputs")
28.
29. #reset new scratch folder to current workspace environment
30. arcpy.env.workspace = "intermediate_outputs"
31. #set scratch variable
32. scratch = arcpy.env.workspace
33.
34. #copy/rename input polygon and fishnet shapefile so attribute head-
    ings will be predictable
35.
36. arcpy.CopyFeatures_management(polygon_input, "snag_polys.shp")
37. arcpy.CopyFeatures_management(fishnet_input, "fishnet_copy.shp")
38.
39. #clip snag_polys and fishnet_copy shapefiles to ROI
40. arcpy.Clip_analysis("snag_polys.shp", roi, "snag_polys_clip.shp")
41. arcpy.Clip_analysis("fishnet_copy.shp", roi, "fishnet_copy_clip.shp")
42.
43. #dissolve snag_polys_clip to get rid of any overlapping features gener-
    ated by afe model
44. arcpy.Dissolve_manage-
    ment("snag_polys_clip.shp", "snag_polys_clip_diss", "", "", "SINGLE_PART")
45.
46. #set these copied/dissolved shapefiles as variables
47. snag_polys = "snag_polys_clip_diss.shp"
48. fishnet_copy = "fishnet_copy_clip.shp"
49.
```

```

50. #run Identity on fishnet ith polygons as identity features saving out-
    put as new shapefile
51. arcpy.Identity_analysis(fishnet_copy, snag_polys, "identity_output.shp")
52.
53. #select lines that cross polygons and make new shapefile
54. arcpy.MakeFeatureLayer_management("identity_out-
    put.shp", "lyr1")
55. arcpy.SelectLayerByAttribute_management("lyr1", "NEW_SELEC-
    TION", ' "FID_snag_p" <> -1 ')
56. arcpy.CopyFeatures_management("lyr1", "lines_on_polygons.shp")
57.
58. #make multipart lines into singlepart
59. arcpy.MultipartToSinglepart_management("lines_on_polygons.shp", "lines_on_poly-
    gons_singlepart.shp")
60.
61. #project to Coordinate system using meters
62. arcpy.Project_management("lines_on_polygons_singlepart.shp", "lines_on_poly-
    gons_singlepart_projected.shp", projection)
63.
64. #add length field
65. arcpy.AddField_management("lines_on_polygons_singlepart_pro-
    jected.shp", "LENGTH", "DOUBLE", 10, 9)
66.
67. #calculate length (in meters, unit of projection in this case)
68. with arcpy.da.UpdateCursor("lines_on_polygons_singlepart_pro-
    jected.shp", ("LENGTH", "SHAPE@LENGTH")) as cursor1:
69.     for row in cursor1:
70.         row[0] = row[1]
71.         cursor1.updateRow(row)
72.
73. #delete lines that are less than desired height/length (to improve pro-
    cessing). First convert height to length
74. min_length = min_height/math.tan(math.radians(angle))
75.
76. with arcpy.da.UpdateCursor("lines_on_polygons_singlepart_pro-
    jected.shp", "LENGTH") as cursor:
77.     for row in cursor:
78.         if row[0] < min_length:
79.             cursor.deleteRow()
80.
81. #summary statistics to find longest segments for each fishnet line, by polygon
82. arcpy.Statistics_analysis("lines_on_polygons_singlepart_projected.shp", "long-
    est_parts", [{"LENGTH", "MAX"}], ("FID_snag_p", "FID_fishne"))
83.
84. #sort fields by FID_of_polygons and then by FID of Fishnet
85. #sorting with ArcGIS INFO tables has a BUG and returns error, so con-
    vert to mdb table, sort, and convert back.
86. #changed table to .gdb on 1/27/15 (5 instances)
87. arcpy.CreatePersonalGDB_management(scratch, "table.mdb")
88. arcpy.TableToTable_conversion("longest_parts", "table.mdb", "longest1")
89. sort_fields = [{"FID_SNAG_P", "ASCENDING"}, {"FID_FISHNE", "ASCENDING"}]
90. arcpy.Sort_management("table.mdb/longest1", "table.mdb/long_s", sort_fields)
91. arcpy.TableToTable_conversion("table.mdb/long_s", scratch, "longest.dbf")
92.
93. #####
94.
95. #Part 2: parsing the lines to find the local maxima fishnet subsets in each pol-
    ygon
96.
97. #set inputs for part 2 and output location
98. input_shapefile = "lines_on_polygons_singlepart_pro-
    jected.shp" #D:\Kevin_Kent_imagery\g_p1b_12a_georftosnags\script_part\interme-
    diate\lines_on_polygons_singlepart_projected.shp"

```

```

99. #the following line was changed from "longest" to "longest.dbf" on 1/27/15
100.     #because 10.2 does not leave it as INFO style table in 2nd TabletoTa-
    ble conversion above
101.     input = "longest.dbf"
102.     output = workspace + "//final_output.shp"
103.
104.     #count number of rows in input table
105.     result = arcpy.GetCount_management(input)
106.     count = int(result.getOutput(0))
107.
108.     #create an array with as many rows as input table. values are zeros.
109.     arr1 = numpy.zeros(shape=(count, 4))
110.
111.     #use search cursor to fill indexable array
112.     i = 0
113.     #Column 0 changed to "OID" from "Rowid" (as well as making long-
    est a .dbf instead of INFO) to accomodate 10.2
114.     with arcpy.da.SearchCursor(in-
    put, ["OID", "FID_SNAG_P", "MAX_LENGTH"]) as cursor:
115.         for row in cursor:
116.             arr1[i,0] = row[0]
117.             arr1[i,1] = row[1]
118.             arr1[i,2] = row[2]
119.             #4th column is left as zeroes for flagging
120.             i +=1 #increments i by 1 with each row
121.
122.
123.     #PARSING to find local maxima fishnet lines in each polygon:
124.     r = 0
125.     #special case for first row
126.     while r < 1:
127.
128.         #checks first row to see if it is from same polygon as next row
129.         if arr1[r,1] != arr1[r+1,1]:
130.             #if different, flags and increments counter
131.             arr1[r,3] = 1
132.
133.         #if from same poly-
    gon, check to see if it has a longer max_length than next
134.         elif arr1[r,2] > arr1[r+1,2]:
135.             #if longer, flags and increments counter
136.             arr1[r,3] = 1
137.
138.         r +=1
139.
140.     #procedure for all but first and last row
141.     while r < (count-1):
142.
143.         #flagging procedure for multiple fishnet lines in one polygon
144.         if arr1[r,1] == arr1[r-1,1] and arr1[r,1] == arr1[r+1,1]:
145.             if arr1[r,2] > arr1[r-1,2] and arr1[r,2] > arr1[r+1,2]:
146.                 arr1[r,3] = 1
147.
148.         #flagging procedure for first fishnet line in a polygon
149.         elif arr1[r,1] == arr1[r-1,1] and arr1[r,1] != arr1[r+1,1]:
150.             if arr1[r,2] > arr1[r-1,2]:
151.                 arr1[r,3] = 1
152.
153.         #flagging procedure for last fishnet line in a polygon
154.         elif arr1[r,1] != arr1[r-1,1] and arr1[r,1] == arr1[r+1,1]:
155.             if arr1[r,2] > arr1[r+1,2]:
156.                 arr1[r,3] = 1
157.

```

```

158.         #flagging procedure for polygon with only one fishnet line
159.         elif arr1[r,1] != arr1[r-1,1] and arr1[r,1] != arr1[r+1,1]:
160.             arr1[r,3] = 1
161.
162.         #increment counter
163.         r +=1
164.
165.         #procedure for last row
166.         if arr1[r,1] == arr1[r-1,1]:
167.             if arr1[r,2] > arr1[r-1,2]:
168.                 arr1[r,3] = 1
169.
170.         #add flag field to input
171.         arcpy.AddField_management(input, "FLAG", "INTEGER", 1)
172.
173.         #run update cursor to change "FLAG" attribute to value in third col-
umn of array
174.         e=0
175.         with arcpy.da.UpdateCursor(input, "FLAG") as cursor:
176.             for row in cursor:
177.                 row[0] = arr1[e,3]
178.                 e += 1
179.                 cursor.updateRow(row)
180.
181.         #delete unflagged rows, should speed up joining time.
182.         with arcpy.da.UpdateCursor(input, "FLAG") as cursor:
183.             for row in cursor:
184.                 if row[0] == 0:
185.                     cursor.deleteRow()
186.
187.
188.         #join gets bogged down if too many fishnet lines, segments, etc
189.         #join table to shapefile
190.         arcpy.JoinField_management(input_shapefile, "length", in-
put, "MAX_LENGTH", "FLAG")
191.
192.         #select flagged features and export to new shapefile
193.         arcpy.MakeFeatureLayer_management(input_shape-
file, "lyr")
194.         arcpy.SelectLayerByAttribute_management("lyr", "NEW_SELEC-
TION", ' "FLAG" = 1 ')
195.         arcpy.CopyFeatures_management("lyr", output)
196.
197.
198.         #add field to ouput for height calculation
199.         arcpy.AddField_management(output, "SNAG_HT", "DOUBLE", 10, 9)
200.
201.         #calculate height of remaining lines using equation Tan(an-
gle) * length = height
202.         with arcpy.da.UpdateCursor(output, ["LENGTH", "SNAG_HT"]) as cursor:
203.             for row in cursor:
204.                 row[1] = math.tan(math.radians(angle)) * row[0]
205.                 cursor.updateRow(row)
206.
207.

```

## Appendix C Snag Detector Tool Directions

Snag\_Detector.tbx

### **Directions for Using .AFE Model for Snag Feature Extraction and for Using Script to Resolve Individual Snags and Adjust Height**

This script was originally created for ArcGIS 10.1 and Python 2.7

#### **Using .AFE Model to Resolve Snag Polygons:**

1. Prepare your image(s) by georeferencing
2. Construct Region of Interest (ROI) polygon
3. Clip image to ROI or slightly larger
4. Using Feature Analyst in ArcGIS, run the Batch Processing module with the provided .AFE model and your image(s).
5. Clip output by mask if desired/necessary
6. Save polygon outputs to desired locations

#### **Using the Script to Resolve Snag Polylines:**

This script provides a novel approach for delineating snag shadow locations from a shapefile with simple (1 shadow - 1 shape) and complex (many shadows – 1 shape) polygons by finding the local maximum lengths of lines running the length of each polygon shape.

This can be done using the results from any desired method that outputs snag shadow features as polygons.

1. Copy the polygon and ROI shapefiles to a working folder
2. Construct a fishnet:
  - A. Buffer your ROI by a distance =  $(.5) * ((\text{longest side of ROI}) - (\text{shortest side of ROI}))$
  - B. In the Data Management Toolbox, Feature Class Folder, select Create Fishnet.
  - C. Set the output.
  - D. Set the template extent to the buffered ROI shapefiles.
  - E. Set the number of Columns to that so the output will have line spacings equal to half that of the width of the snag polygons (this may take some trial and error, spacing was 0.2m in original method utilizing 1:12000 imagery)
  - F. Use the Editing toolbar edit the fishnet shapefile.
  - G. Select all the features in the fishnet shapefile and click the rotate button.
  - H. Do not use the cursor to rotate. Click the “a” key and a window will open prompting a rotation angle
  - I. Rotate until the fishnet lines are in alignment with the directions of the shadows. For example, if the image was taken at 9:00 AM (non-Daylight Savings Time) on the spring equinox, you would expect the angle of rotation to be around 120 degrees (give or take a few depending on the positioning in the time zone). Record the final angle of rotation (azimuth).
  - J. Save edits.

3. Make sure the Custom Find\_Snags Toolbox and its accompanying python (.py) script, local\_maxima\_snag\_script, is saved to a local directory.
4. Add this Toolbox to the default list of Toolboxes in ArcGIS.
5. Edit the Toolbox so the source information directs to the downloaded python script.
  
6. Go to the US Naval Observatory's Sun or Moon Altitude/Azimuth Table (<http://aa.usno.navy.mil/data/docs/AltAz.php>) and using Form B, select measurements for the sun, enter the year and date the source imagery was taken, as well as it's latitude and longitude, and set the tabular interval to 1 minute. (You can set the time zone if you like but it is not necessary).
7. Find the altitude (angle of elevation) that corresponds to the azimuth (angle of rotation) that was recorded in step 2.I. Record this number.
  
8. Finally Run the Find\_Longest\_Snags scripting tool in ArcGIS
  - A. Set the inputs for the working folder, the snag polygon shapefile, the rotated fishnet shapefile, the ROI, and the projection file (you might need to find the correct projection file in ArcCatalog and save it to the working folder beforehand).
  - B. Set the angle to the altitude angle derived in step 7.
  - C. Use the slider to pick a (unadjusted) minimum height for the output snags. A higher minimum will speed processing time by eliminating short lines that are most likely noise.

9. When script finishes, the working folder will contain a shapefile called `final_output` showing polylines of snag shadow locations with attributes for each feature estimating the height of each snag.

10. (Optional). If you wish to perform a height adjustment, open the attribute table of `final_output` and click "Add Field." Create a new field as type: Double and set the precision and accuracy to the desired length. Right click on the new field and open "Field Calculator." In the code box write:

```
[SNAG_HT] * Adjustment_factor
```

The adjustment factor is a number of your choosing; this number can be inferred by using ground truth data or different remote measurement techniques.